JOURNAL of the MEXICAN CHEMICAL SOCIETY

https://www.jmcs.org.mx/

Article

Open Access

J. Mex. Chem. Soc. **2026**, *70(1):e2576*

Received October 29th, 2025
Accepted May 13th, 2026

http://dx.doi.org/10.29356/jmcs.v70i1.2576
e-location ID: 2576

Keywords:
QTAIM, ELF, NCI, IRI, hydrogen-bonding interactions, trichlorozincate, amino amides

Palabras clave:
QTAIM, ELF, NCI, IRI, interacciones puente de hidrógeno, triclorozincato, amino amidas

***Corresponding author:**
Eltonh Islas Trejo;
Antonio Rafael Tapia Benavides
email: eltonh_islas@uaeh.edu.mx;
tapiab@uaeh.edu.mx

ISSN-e 2594-0317

Intramolecular C–H•••Cl Interactions in Amino Amide Trichlorozincates Confirmed by Electron Density Topology

Eltonh Islas Trejo[1*], Angela Margarita Tlahuextl Romero[2], Antonio Rafael Tapia Benavides[2*]

[1]Preparatoria No. 3, Universidad Autónoma del Estado de Hidalgo, 42030, Pachuca, Hidalgo, México.
[2]Área Académica de Química, Universidad Autónoma del Estado de Hidalgo, 42184, Pachuca, Hidalgo, México.

Abstract. In this work, we used QTAIM, ELF topological electron density analysis, NCI, and IRI methodologies to study the presence of intramolecular C–H•••Cl interactions in trichlorozincates derived from amino amides. Bond paths (BP) are present between the chlorines of $ZnCl_3^-$ group with the aliphatic H10 and aromatic H4 hydrogens respectively in compounds 1 and 2. ρ_b and δ(H,Cl) values indicated that the hyperconjugative component $n(Cl3)\rightarrow\sigma^*_{C10–H10}$ is more significant in compound 1 than in 2. Likewise, H4•••Cl2 interactions have ρ_b values near the lower limit of the range reported by Koch and Popelier for C-H•••X hydrogen bondings. Additionally, the great ellipticity (ε) > 1 of bond $CP_{H4\cdots Cl2}$ predicts the vanish of the $BP_{H4\cdots Cl2}$ with a small change in the molecular geometry of compound **1**. Again, λ_1 and λ_2 values show that C10–H10B•••Cl3 hydrogen bonding is more stable in compound 1 than the other intramolecular C–H•••Cl interactions present in compounds 1 and 2. The source function (SF) suggests that a methyl group at C10 contributes to weakening the H10•••Cl3 interactions. The enveloped plot of $\nabla^2\rho_b$ confirms a higher charge concentration between the H10B and Cl3 attractors in compound 1 compared to 2. Finally, ELF analysis showed that C–H•••Cl interactions decrease the volume of the monosynaptic basin V(H).

Article

J. Mex. Chem. Soc. **2026**, *70(1):e2576*
Regular Issue

ISSN-e 2594-0317

Resumen. En este trabajo, nosotros usamos las metodologías de la topología de la densidad electrónica QTAIM, ELF, NCI, e IRI metodologías para estudiar las interacciones intramoleculares C-H•••Cl en tetraclorozincatos derivados de amino amidas. Caminos de enlace (BP) están presentes entre los cloros del grupo $ZnCl_3^-$ con los hidrógenos alifáticos H10 y los hidrógenos aromáticos H4 respectivamente en los compuestos 1 y 2. Los valores de ρ_b y δ(H,Cl) indicaron que el componente hipercojugativo n(Cl3)→σ*$_{C10–H10}$ contribuye de manera más significativa en 1 respecto a 2. Asimismo, las interacciones H4•••Cl2 tienen valores de ρ_b cercanos al límite inferior del rango reportado por Koch and Popelier para los puentes de hidrógeno C-H•••X. Adicionalmente, la gran elipticidad (ε) > 1 de CP$_{H4•••Cl2}$ predice el desvanecimiento del BP$_{H4•••Cl2}$ en 1 con un pequeño cambio en la geometría de la molécula. Una vez más, los valores λ_1 y λ_2 muestran que el puente de hidrógeno C10–H10B•••Cl3 de 1 es la interacción intramolecular C–H•••Cl más estable en 1 ó 2. La función fuente (SF) sugiere que la presencia de un grupo metilo en C10 contribuye al debilitamiento de las interacciones H10•••Cl3. El diagrama envolvente de $\nabla^2\rho_b$ confirma una mayor concentración de carga entre los atractores H10B y Cl3 en 1 respecto a 2. Finalmente, el análisis ELF mostró que las interacciones C-H•••Cl disminuyen el volumen de la cuenca monosináptica V(H).

Introduction

Hydrogen bonds (X–H•••Y) play a crucial role in the structure, function, and conformational dynamics of biomolecules. [1] These non-covalent interactions are highly relevant to modern chemistry, as they promote polymer assembly, the design of molecular cages, and the operation of host–guest systems. [2] Hydrogen bonds can be classified as classical or non-classical. [3] Classical hydrogen bonds are strong interactions in which the donor atom X is highly electronegative (e.g., O–H•••O, N–H•••O, N–H•••N). In contrast, non-classical hydrogen bonds involve less electronegative donor atoms (such as C–H, Si–H, P–H) and are therefore weaker. [4–5] The hydrogen bonding behavior of C–H systems as hydrogen bond donors was initially recognized by molecular biologists, who highlighted their importance in stabilizing the secondary structure of biomolecules. [6] C–H hydrogen bonds occur when the carbon atom is bonded to electron-withdrawing groups, as is the case in peptides, aromatic rings, triazoles, and related systems. [7–8] In particular, C–H•••Cl hydrogen bonds have gained significant attention due to their role in substrate activation in metalloenzymes, drug polymorphism, anion–receptor interactions, and sensor design, among others. [6, 9–10] However, the experimental identification of C–H•••Cl interactions based on geometric and spectroscopic parameters can be ambiguous. This behavior is due to a delicate balance between hyperconjugative effects that lengthen C–H bonds and polarization effects that shorten them. [5] As a result, the experimental determination of such interactions is not always straightforward or conclusive. The low electronegativity of carbon cause weak C-H•••Cl interactions, making it difficult to distinguish between these and hydrogen bonds or van der Waals interactions. Crystallographic studies have shown that C-H•••Cl-M systems preferentially form hydrogen bonds, whereas the C-H•••Cl-C interactions correspond to van der Waals close packing. [11] Structural studies facilitate the characterization of the intermolecular C-H•••Cl interactions because there are not apparent geometrical restrictions that prevent their directional behavior, and they tend to have linear geometries. The correct assignment of intramolecular interactions is challenging because these interactions are integral to the molecular conformation. In this context, we characterized the intramolecular C-H•••Cl interactions in coordination compounds **1** and **2**. In these molecules the chlorine atoms are bonded to zinc and close to adjacent hydrogen atoms. Thus, it is interesting to determine if the presence of the $ZnCl_3^-$ group contributes to the conformation of the organic fragment by means of weak intramolecular interactions or if its molecular geometry is product of close packing phenomena.

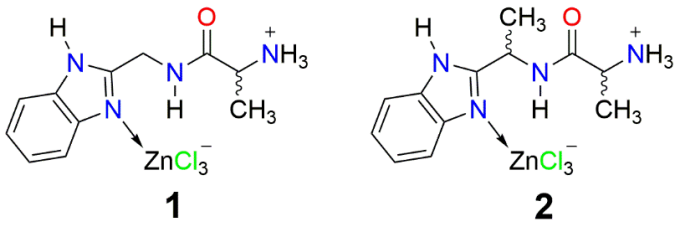

Scheme 1. Amino amide trichlorozincates **1** and **2**.

J. Mex. Chem. Soc. **2026**, *70(1):e2576*
Regular Issue

ISSN-e 2594-0317

Spectroscopic studies provide evidence for the possible presence of C–H•••Cl hydrogen bonds in coordination complexes **1** and **2** (Scheme 1). [12–13] However, crystallographic data reveal C•••Cl longer distances than the sum of the van der Waals radii of carbon (1.70 Å) and chlorine (1.80 Å), as reported by Pauling and Bondi. [14] Although the van der Waals distance criterion is discouraged by IUPAC, C•••Cl longer distances than 3.5 Å raise doubts about the nature of the C–H•••Cl contacts. This dubiety is because the van der Waals rule is generally valid for strong hydrogen bonds, whose attractive interaction has a significant covalent character. [15] It has been proposed that C–H•••Cl interactions are predominantly electrostatic in nature. [16] Nevertheless, there are systems in which non-electronegative carbon atoms participate in hydrogen bonding interactions. [17] In such cases, the commonly accepted van der Waals radius of hydrogen (1.2 Å) may be underestimated, and longer values than 1.2 Å may be more appropriate. [18] Therefore, hydrogen bonds with C•••Cl distances exceeding 3.5 Å are plausible. In light of these inconsistencies, non-covalent interactions can be further evaluated and characterized using the quantum theory of atoms in molecules (QTAIM) and the electron localization function (ELF). [13, 19-21] The presence of bond critical points (3,-1) between hydrogen atoms and hydrogen bond acceptors is one of the criteria recommended by IUPAC to confirm the existence of attractive X–H•••Y intra- or intermolecular interactions. [18] Therefore, the identification of C–H•••Cl contacts is not based solely on the presence of bond paths, but on a consistent evaluation of multiple descriptors. This integrated approach is consistent with recent studies showing that the combined use of QTAIM, ELF, and complementary real-space methods provides a more reliable characterization of non-covalent interactions as NCI and IRI methods. [22-24]

In the present study, we employed the crystallographic structures of amino amide trichlorozincates **1** and **2**, as reported by Islas-Trejo et al., to perform a topological analysis of the electron density. [12] The organic fragments of compounds **1** and **2** are amino amides derived from glycine and alanine, respectively, and can thus be considered structural analogs of dipeptides. The coordination of benzimidazolic nitrogen to the trichlorozincate group ($ZnCl_3^-$) enables the investigation of intramolecular non-covalent C–H•••Cl interactions and provides molecular models relevant to macromolecular systems. Within the framework of the Quantum Theory of Atoms in Molecules (QTAIM), we determined the electron density of the intramolecular C–H•••Cl interactions in compounds **1** and **2**. We applied the criteria proposed by Koch and Popelier to characterize these interactions. [25] Additionally, we confirmed the presence of such interactions through a topological analysis of the electron localization function (ELF), non-covalent interaction (NCI), and interaction region indicator (IRI) methods. [21-26]

Methodology

Computational details

The geometries of compounds **1** and **2** were obtained from the CIF files CCDC 2183163 and CCDC 2183174, published in the Cambridge Crystallographic Data Centre and included as supporting material in reference 12. [27, 12] The wavefunctions of **1** and **2** were generated via single-point calculations on the experimental geometries using the *Gaussian 03* package at the B3LYP/6-311++G(2d,2p) level of theory. [28] QTAIM analysis was performed using the AIMALL program. [29] ELF studies were carried out with the Multiwfn software, and ChimeraX was used to visualize the localization domains of η(r). [30–31]

Results and discussion

The interaction between two atoms results in the formation of a line of maximum density linking the nuclei of the two atoms which is known as a bond path (**BP**). [20] Figures 1 and 2 display the molecular graphs (networks of **BP**s connecting neighboring atomic nuclei) of compounds **1** and **2**. In these graphs, **BP**s are represented by black lines. Each BP contains a minimum in electron density known as a bond critical point (**BCP**). In the molecular graphs of compounds **1** and **2**, the **BCP**s are indicated by green dots. In the molecular graph, the **BP**s corresponding to weak interactions are represented by black dashed lines. Thus, it can be

http://dx.doi.org/10.29356/jmcs.v70i1.2576

J. Mex. Chem. Soc. **2026**, *70(1):e2576*
Regular Issue

ISSN-e 2594-0317

confirmed that attractive interactions between H4•••Cl2 and H10B•••Cl3 are present in coordination compounds **1** and **2**.

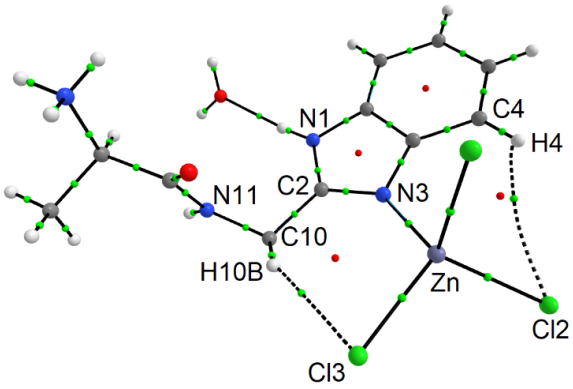

Fig. 1. Molecular graph of compound **1** determined by electron density topology. Green dots indicate bond critical points (**BCP**s, 3,-1). Red dots represent ring critical points (**RCP**s, 3,+1), indicating the presence of a ring.

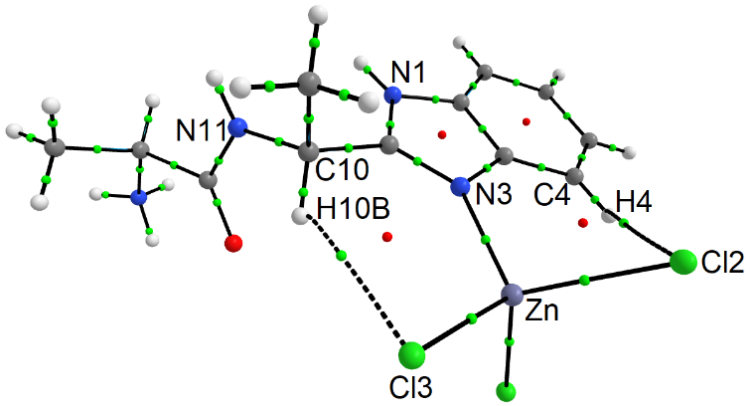

Fig. 2. Molecular graph of compound **2** determined by electron density topology. Green dots indicate bond critical points (**BCP**s, 3,-1). Red dots represent ring critical points (**RCP**s, 3,+1), indicating the presence of a ring.

Every **BCP** is defined by three eigenvalues (λ_1, λ_2, λ_3) of the electron density (ρ). [19] The eigenvalue λ_3 describes the curvature of ρ along the bond path and is positive. In contrast, λ_1 and λ_2 are negative and represent the negative curvatures of ρ perpendicular to the bond path. [32] For this reason, every **BCP** is topologically described as a (3,-1) critical point. [18] The sum of λ_1, λ_2, and λ_3 defines the Laplacian of ρ at the **BCP**, denoted as $\nabla^2\rho_b$. Negative values of $\nabla^2\rho_b$ indicate a local concentration of electron density between two attractors, which is characteristic of covalent interactions. [33] Furthermore, the ellipticity $\varepsilon = \lambda_1/\lambda_2 - 1$ indicates the extent to which ρ at the **BCP** is elliptical. A minimum value of ε = 0 corresponds to σ density, whereas values close to one are associated with π density. [32]

QTAIM studies reveal the presence of two intramolecular C–H•••Cl interactions in coordination compounds **1** and **2** (figures 1 and 2). Closed-shell bonding interactions (such as hydrogen bonds and van der Waals) are characterized by positive Laplacian values and low electron density at the bond critical point (3,-1). [34] For comparison with well-established classical hydrogen bonds, earlier topological studies report that the

http://dx.doi.org/10.29356/jmcs.v70i1.2576

J. Mex. Chem. Soc. **2026**, *70(1):e2576*
Regular Issue

ISSN-e 2594-0317

water dimer (O-H•••O) exhibits ρ_b values next to 0.02 a.u. and positive Laplacian ($\nabla^2\rho_b \approx 0.06$ a.u) consistent with a classical hydrogen bond. [35] In contrast, non-classical hydrogen bonds, such as C-H•••O interactions, display ρ_b values that fall within the range of 0.002-0.034 a.u. and broader angular distributions. [25] The interactions C4-H4•••Cl2 and C10-H10B•••Cl3 in compounds **1** and **2** display ρ_b values that fall within the range reported by Koch and Popelier for hydrogen bonds (Table 1). [25]

Table 1. Delocalization and Bond Indices of Compounds **1** and **2.** [25,35]

Interaction	ρ_b	$\nabla^2\rho_b$ [c]	**δ(H,Cl)**	**ε**
Compound **1**				
C4-H4•••Cl2	0.004	0.014	0.000	2.193
C10-H10B•••Cl3	0.012	0.036	0.224	0.073
Compound **2**				
C4-H4•••Cl2	0.006	0.020	0.035	0.362
C10-H10B•••Cl3	0.008	0.026	0.047	0.039

Furthermore, it is observed that the magnitude of ρ_b in compound **1** is three times higher for the C10–H10B•••Cl3 interaction (ρ_b = 0.012 a.u.) compared to the value obtained for C4–H4•••Cl2 (ρ_b = 0.004 a.u.). The ρ_b value for the C10–H10B•••Cl3 hydrogen bond is similar to that of interactions in which electronegative groups are directly bonded to the carbon atom. [25] This behavior aligns with the 19 cm^{-1} red shift observed in the methylene scissoring vibration of compound **1**. [11] This result indicates elongation of the C–H bond and suggests that the hyperconjugative interaction n(Cl3) → σ*C10–H10 dominates the interaction, leading to an accumulation of electron density in the internuclear region. [5, 36] Bader states that the delocalization index δ(A,B) provides a measure of the number of α,β electron pairs exchanged between the basins of atoms A and B and serves as a physical indicator of covalency. [34] The δ(H10B,Cl3) value of 0.224 indicates a polar interaction with a significant covalent component. Increased sharing of electron density between the H10B and Cl3 basins results in a decrease of the delocalization index for the C10–H10B bond compared to C10–H10A. Hydrogen atom H10A does not participate in hydrogen bonding, and its delocalization index δ(C10–H10A) is 0.94, similar to that of C–H bonds in ethane. [37] In contrast, the delocalization index δ(C10–H10B) is 0.88, supporting the presence of hyperconjugative effects in the C10–H10B•••Cl3 interaction.

On the other hand, the delocalization index for the C4–H4•••Cl2 interaction is effectively zero, indicating that no α,β electron pairs are exchanged between the H4 and Cl2 basins. [36] The intramolecular C4–H4•••Cl2 interaction gives rise to a ring critical point (**RCP**, 3,+1). As shown in Fig. 1, the bond path is curved inward into the ring, and the distance between the **BCP** and **RCP** is very short. The proximity of these two critical points, along with the high ellipticity value for the **BP** of C4–H4•••Cl2 (ε = 2.192), suggests that a change in molecular geometry could lead to the coalescence of the **BCP** and **RCP** and the subsequent disappearance of the H4•••Cl2 bond path. [36]

The C4–H4•••Cl2 and C10–H10B•••Cl3 interactions in compound **2** exhibit similar ρ_b values (0.006 and 0.008 a.u., respectively), but these are close to the lower electron density limits proposed by Koch and Popelier for hydrogen bonding interactions. [25] Moreover, the electronic delocalization between the chlorine and hydrogen atoms in these interactions is between five and six times smaller than that found for the C10–H10B•••Cl3 interaction in compound **1**. This behavior is consistent with the absence of a red shift in the C10–H10 stretching vibration reported by Islas-Trejo et al. for compound **2**, In contrast, coordination compound **1** exhibits a significant red shift (11 cm^{-1}). [12] The magnitudes of ρ_b and δ indicate that these interactions in compound **2** correspond to very weak hydrogen bonds.

J. Mex. Chem. Soc. **2026**, *70(1):e2576*
Regular Issue

ISSN-e 2594-0317

Furthermore, as λ_2 becomes more negative, the charge concentration between the attractors increases, leading to a more stable system. Thus, λ_2 is 1.8 times more negative in the C10–H10B•••Cl3 interaction of compound **1** (–0.0098) compared to compound **2** (–0.0054). This phenomenon can be observed in the Laplacian isosurface plots of compounds **1** and **2** (Fig. 3). At the isovalue L(r) = 0.03, the greater charge concentration between the attractors H10B and Cl3 in compound **1** compared to compound **2** is confirmed. This result demonstrates that the stabilizing components (λ_1 and λ_2) of the C10–H10B•••Cl3 interaction are more pronounced in compound **1** than in compound **2**.

Table 2. Atomic Charges and Source Function (**SF**) in Intramolecular C–H•••Cl Interactions in Compounds **1** and **2.** [38,39]

Interaction	***q*(C)**	***q*(H)**	***q*(Cl)**	**%SF**
Compound 1				
C4-H4•••Cl2	0.200	0.069	-0.727	
C10-H10B•••Cl13	0.515	0.071	-0.730	24.1
Compound 2				
C4-H4•••Cl2	0.205	0.089	-0.707	
C10-H10B•••Cl13	0.418	0.011	-0.718	4.6

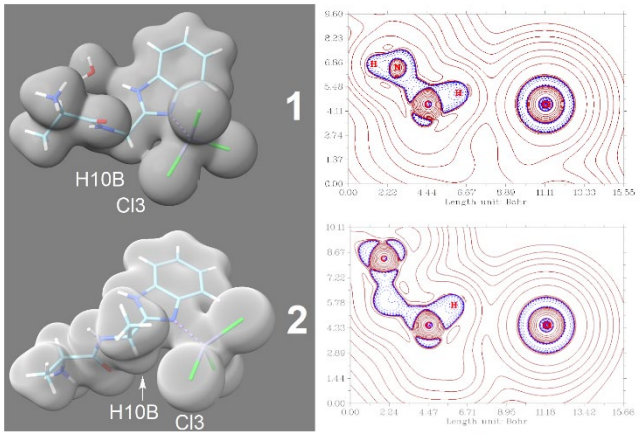

Fig. 3. (A) Isosurface plot of the Laplacian distribution for compounds **1** and **2**. The L(r) = 0.03 surface shows that charge concentration regions are shared between H10B and Cl3 in compound **1**, but not in compound **2**. **(B)** maps cut in the C10-H10B-Cl3 plane of the molecule. Dotted blue lines mark regions of charge accumulation (negative $\nabla^2\rho_b$) while solid red lines mark regions of charge depletion (positive $\nabla^2\rho_b$).

The difference in the magnitude of ρ_b for the C10–H10B•••Cl3 interaction between compounds **1** and **2** can be attributed to the presence of a methyl group bonded to C10 in compound **2**. The contribution to the magnitude of ρ_b from atoms and/or functional groups located at positions distant from the C–H•••Cl interaction can be quantified using the percentage source function (%**SF**) (Table 2). [20, 39-40] Thus, the ρ_b magnitude for

http://dx.doi.org/10.29356/jmcs.v70i1.2576

J. Mex. Chem. Soc. **2026**, *70(1):e2576*
Regular Issue

ISSN-e 2594-0317

the H10B•••Cl3 interaction receives a greater contribution from the hydrogen atom H10A [%**SF** = 24.1 %] in compound **1** compared to the methyl group attached to C10 [%**SF** = 4.6 %] in compound **2**. This phenomenon is related to the electron-donating capacity of substituent groups attached to carbon C10. Therefore, the **SF** value indicates that the presence of a methyl group at C10 weakens the H10•••Cl3 interaction. **SF** values record the changes in the H-basin, the increase in electronegativity of donor and acceptor atoms, increases the ρ_b magnitude. [39] Moreover, Gatti found that **S**% (H) values indicate the nature of the hydrogen bonding interactions. [40] Thus, the source values for H10B [**S**% (H10B) = -75 % for compound **1** and -12 % for compound **2**] are in concordance with the electrostatic nature of the C10-H10B•••Cl3 interactions. The highly negative **S**% (10B) value in **1** confirms the predominance of charge transference phenomena in this interaction. On the other hand, the **S**% (H) value is positive in those interactions where donors are very polarized, such as carboxylic acids and hydronium ions. [40]

Additionally, the atomic charges of the hydrogens involved in the C–H•••Cl interactions reveal that in compound **1**, the C10–H10B•••Cl3 interaction induces polarization of the C–H bond (Table 2). [5] In contrast, in compound **2**, the positive charge on the hydrogen involved in the C10–H10•••Cl3 interaction is six times smaller than in compound **1**, although without significant electronic transfer. Complementarily, the electron localization function (ELF) of the electron density allows for the classification of chemical bonds. [41] According to Silvi, ELF analysis provides a molecular description consistent with the Lewis model, enabling a chemical interpretation of the attractors and basins present in a system. [21] The graphical representation of the ELF delineates the volumes of basins where Pauli repulsion is weak. When a hydrogen bond interaction forms, the volume of the monosynaptic basin of the involved hydrogens tends to decrease. [21] Thus, in Fig. 4, it can be observed that the V(H10A) basin is twice as large as the V(H10B) basin in compound **1**. The volume of V(H10A) (~1.999 Å^3) is similar to that of the basins of the hydrogens in the methyl group (~2.000 Å^3) in compound **1**. In contrast, the volume of V(H10B) (0.962 Å^3) is close to that of the V(H) basins of ammonium hydrogens involved in polar covalent N–H bonds (~1.091 Å^3). The volume of the V(H10) basin in compound **2** is also smaller (1.106 Å^3) than the monosynaptic basins of methylene hydrogens. This difference corroborates the presence of the C10–H10•••Cl3 hydrogen bond in compound **2**, although the basin volume (VH) predicts a weaker H•••Cl interaction in **2** compared to compound **1**. Also, the getting of an A-H•••B complex can change the basin number and the synaptic order. Thus, in strong hydrogen bondings, the disynaptic V(A,H) split results in monosynaptic V(A) and V(H) basins. Nevertheless, these changes do not occur in weak interactions. [21] The core-valence bifurcation index (CVBI) determines if an A-H•••B complex can be considered as a single chemical specie due to the electronic delocalization between V(A,H) and V(B) basins. [42] CVBI presents an almost linear correlation with the binding energy of these non-covalent interactions, and allow distinguishing the strength of A-H•••B complexes. CVBI exhibits positive values in weak interactions, such as F-H•••N_2 (0.102) or Cl-H•••CH_4 (0.074). In contrast, hydrogen bonding has negative CVBI as F-H•••NH_3 (-0.081). [43] C10-H10B•••Cl3 interactions have positive CVBI values in compounds **1** and **2**, and they are weak interactions. But, the CVBI is smaller in **1** (0.058) than in **2** (0.077), and this fact corroborates that the C10-H10B•••Cl3 interaction is stronger in compound **1**.

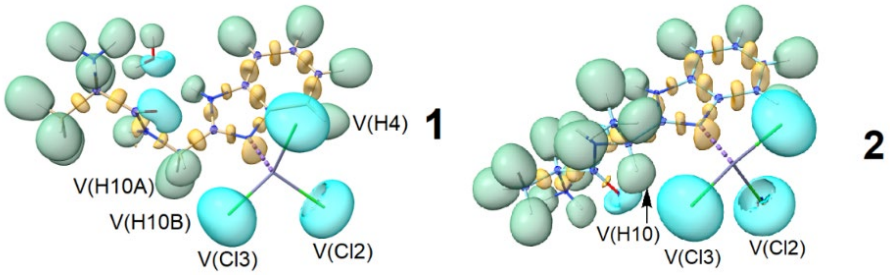

Fig. 4. Localization domains of η(r) for compounds **1** and **2**. The color code for the localization domains is as follows: blue for lone electron pairs [V(Cl), V(N), and V(O)]; green for hydrogen-related domains [V(H)]; orange for bonding domains [V(C,C) and V(C,N)]; and dark blue for core domains [C(C), C(N), and C(Cl)].

http://dx.doi.org/10.29356/jmcs.v70i1.2576

J. Mex. Chem. Soc. **2026**, *70(1):e2576*
Regular Issue

ISSN-e 2594-0317

The non-covalent interaction (NCI) maps show the presence of non-covalent interactions in compounds **1** and **2** (A in Figs. 5 and 6). [26] In scatter map between RDG and *sign*(l_2)*r* , five spikes can be found that disclose the nature of these interactions (B in Figs. 5 and 6). The blue spike indicates the existence of H-bonding interactions. At the same time, green spikes reveal the presence of van der Waals interactions in both compounds. Moreover, brown and red spikes indicate the existence of electronic repulsion zones in these zinc compounds. Thus, in the NCI map of **1**, the blue flattened disc correspond to an H-bonding interaction between the imidazolic N-H donator and the oxygen of a water molecule (A in Fig. 5).

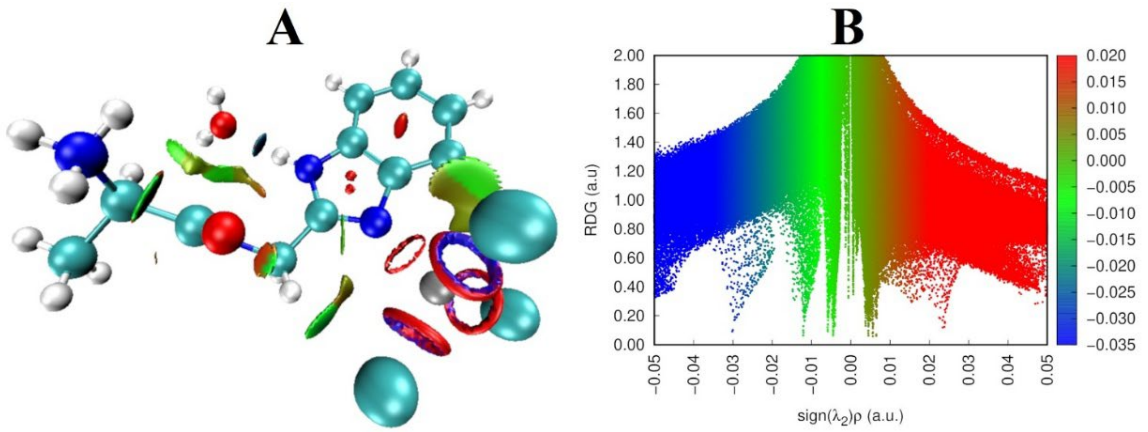

Fig. 5. (A) NCI map of compound **1** of RDG = 0.5, **(B)** Scatter map between RDG and *sign*(l_2)*r* of the grid points of NCI analysis of compound **1**.

According to the NCI analysis, the C-H•••Cl interactions can be classified as van der Waals type in compounds **1** and **2**. However, brown isosurfaces, corresponding to steric repulsion zones, surround the attractive green stains. Whereas the green area due to C10–H10B•••Cl3 interaction is larger than the brown zones in compound **1** (A in Fig. 5), the isosurface area corresponding to repulsion zones is longer in compound **2** (A in Fig. 6). This behavior indicates that C10–H10B•••Cl3 interactions contribute significantly to the conformation of compound **1**. On the other hand, the larger brown zones indicate that the steric phenomena govern the conformation of **2**.

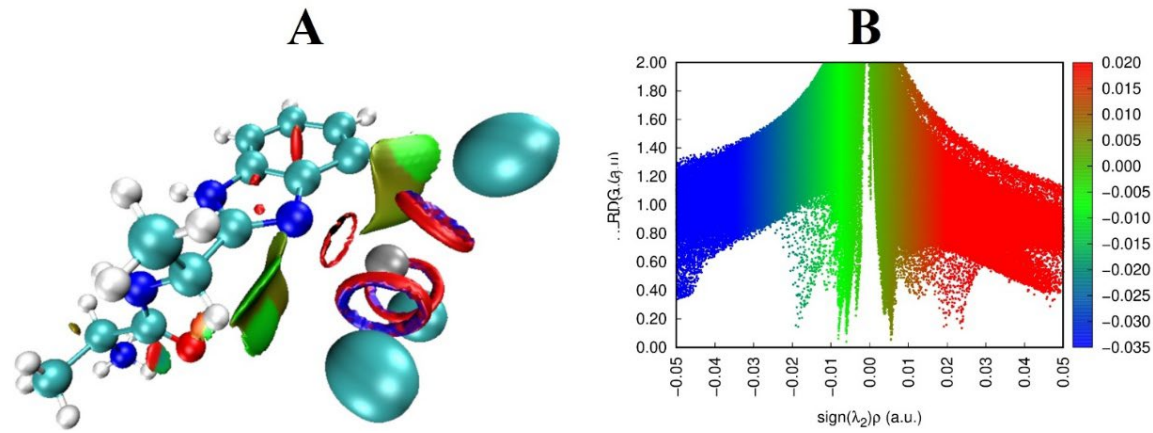

Fig. 6. (A) NCI map of compound **2** of RDG = 0.5, **(B)** Scatter map between RDG and *sign*(l_2)*r* of the grid points of NCI analysis of compound **2**.

http://dx.doi.org/10.29356/jmcs.v70i1.2576

J. Mex. Chem. Soc. **2026**, *70(1):e2576*
Regular Issue

ISSN-e 2594-0317

The interaction region indicator (IRI) shows chemical bonds and weak interactions at the same time. [44] Similar than NCI, the $sign(l_2)r$, and the graphical representation, identify the nature of these interactions. In figures 7 and 8, it can be seen that covalent and Zn-N coordinated bonds are represented as blue isosurfaces. N-H•••O and C10-H10B•••Cl3 are present as flattened discs, indicating localized and directional non-covalent interactions in compound **1** (Fig. 7). However, while the N-H•••O interaction is blue (strong hydrogen bonding), the C10-H10B•••Cl3 is yellowish green (weak hydrogen bonding).

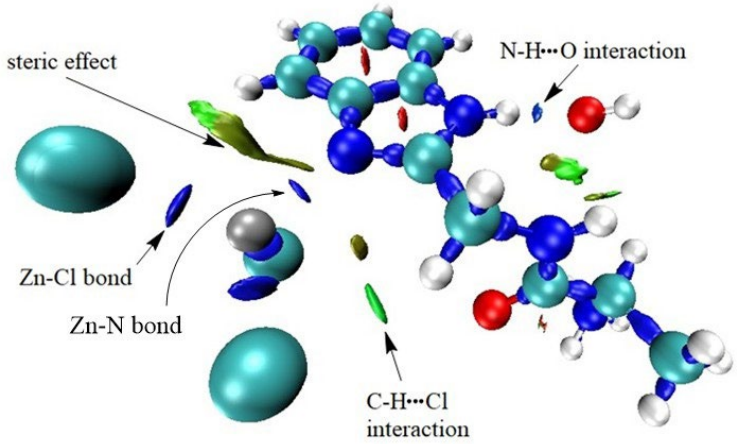

Fig. 7. IRI map of compound **1**. Isovalue of IRI is set to 1.0 a.u.

The IRI map shows green extended stains in compounds **1** and **2**. These spots indicate the presence of non-directional attractive interactions corresponding to van der Waals interactions. This behavior is observed in C4-H4•••Cl2 in compounds **1** and **2**, and C10-H10B•••Cl3 interactions in compound **2**. The presence of directional and non-directional interactions is in concordance with the geometry of these compounds. [12] The bond angle in C10-H10B•••Cl3 tends to linearity in compound **1** [151.9° (2)] and complies with the requirements proposed by the IUPAC, in which hydrogen bonds should preferably be above 110°. [45] However, the bond angle of C10-H10B•••Cl3 interaction in compound **2** [128.6° (2)] is in agreement with the low ρ_b (0.008 a.u.) and l_2 (-0.005) values for a non-directional interactions.

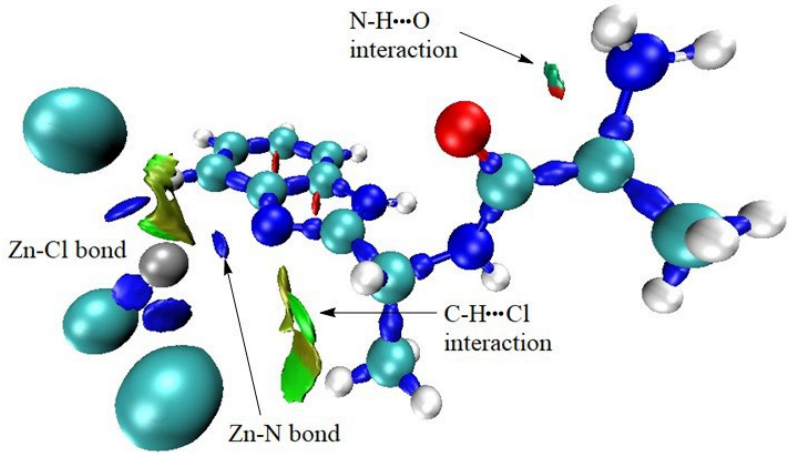

Fig. 8. IRI map of compound **2**. Isovalue of IRI is set to 1.0 a.u.

http://dx.doi.org/10.29356/jmcs.v70i1.2576

J. Mex. Chem. Soc. **2026**, *70(1):e2576*
Regular Issue

ISSN-e 2594-0317

Conclusions

The topological analysis of the electron density confirmed the presence of intramolecular C–H•••Cl interactions in compounds **1** and **2**. The presence of bond paths between H and Cl atoms demonstrates the existence of these interactions. However, the magnitudes of ρ_b and δ(H,Cl) indicate that the hyperconjugative component n(Cl3)→σ*C10–H10 is more significant in compound **1** than in compound **2**. Additionally, the ellipticity of **BCP**_H4•••Cl2 in compound **1** exceeds one, predicting that a small change in the molecular geometry may lead to the disappearance of the H4•••Cl2 bond path.

The source function (**SF**) value reveals that the presence of a methyl group at C10 contributes to the weakening of the H10•••Cl3 interaction. The highly negative **S**% (10B) value in **1** confirms the predominance of charge transference phenomena in C10–H10B•••Cl3 interaction. The Laplacian isosurface map of the electron density for compounds **1** and **2** confirms a greater charge concentration between the H10B and Cl3 attractors in compound **1**. ELF analysis showed that the presence of a C–H•••Cl interaction contributes to a decrease in the volume of the monosynaptic basin V(H). Moreover, CVBI values corroborated that the C10-H10B•••Cl3 is stronger in compound **1**. NCI studies indicate that C10–H10B•••Cl3 interactions contribute significantly to the conformation of compound **1**, but the steric phenomena govern the conformation of **2**. The IRI maps show that C10-H10B•••Cl3 is a directional interaction in compound **1**, but it corresponds to van der Waals interactions (non-directional) in compound **2**.

Acknowledgements

This study was supported by SEP-CONACyT [grant CB-2011/169010]. E.I.T. thanks CONACyT for providing the scholarship (764220).

References

1. Herschlag, D.; Pinney, M. *Biochem.* **2018**, *57*, 3338-3352. DOI: https://doi.org/10.1021/acs.biochem.8b00217
2. Thompson, A. L.; White, N. G. *Chem. Soc. Rev.* **2023**, *52*, 6254-6269. DOI: https://doi.org/10.1039/D3CS00516J
3. Karas, L. J.; Wu, C. H.; Das, R.; Wu, J. I. *Wiley Interdiscip. Rev. Comput. Mol. Sci.* **2020**, *10*, e1477. DOI: https://doi.org/10.1002/wcms.1477
4. Moro, A. C.; Watanabe, F. W.; Anannias, S. R.; Mauro, A. E.; Netto, A. V. G.; Lima, A. P. R.; Ferreira, J. G.; Santos, R. H. A. *Inorg. Chem. Commun.* **2006**, *9*, 493-496. DOI: https://doi.org/10.1016/j.inoche.2006.02.012
5. Alabugin, I. V.; Manoharan, M.; Peabody, S.; Weinhold, F. J. *Am. Chem. Soc*. **2003**, *125*, 5973-5987. DOI: https://doi.org/10.1021/ja034656e
6. Tresca, B. W.; Zakharov, L. ZN.; Carroll, C. N.; Johnson, D. W.; Haley, M. M. *Chem. Commun.* **2013**, *49*, 7240-7242. DOI: https://doi.org/10.1002/anie.201605757
7. Scheiner, S. *J. Indian Inst. Sci*. **2020**, *100*, 61-76. DOI: https://doi.org/10.1007/s41745-019-00142-8
8. Castro, M.; Nicolás-Vázquez, I.; Zavala, J. I.; Sánchez-Viesca, F.; Berros, M. *J. Chem. Theory Comput.* **2007**, *3*, 681-688. DOI: https://doi.org/10.1021/ct600336r
9. Shanahan, J. P.; Mullis, D. M.; Zeller, M.; Szymczak, N. K. *J. Am. Chem. Soc.* **2020**, *142*, 8809-8817. DOI: https://doi.org/10.1021/jacs.0c01718
10. Liu, M.; Yin, C.; Chen, P.; Zhang, M.; Parkin, S.; Zhou, P.; Li, T.; Yu, F.; Long, S. *CrysEngComm.* **2017**, *19*, 4345-4354. DOI: https://doi.org/10.1039/c7ce00772h
11. Thallapally, P. K.; Nangia, A. *CrystEngComm.* **2001**, *27*, 1-6. DOI: 10.1039/b102780h

J. Mex. Chem. Soc. **2026**, *70(1):e2576*
Regular Issue

ISSN-e 2594-0317

12. Islas-Trejo, E.; Tlahuextl, M.; Lechuga-Islas, V. D.; Falcón-León, M.; Tlahuext, H.; Tapia-Benavides, A. R. *J. Mol. Struct.* **2023**, *1274*, 134451. DOI: https://doi.org/10.1016/j.molstruc.2022.134451
13. Arunan, E.; Desiraju, G. R.; et al., *Pure Appl. Chem.* **2011**, *83*, 1637-1641. DOI: https://doi.org/10.1351/PAC-REC-10-01-02
14. Batsanov, S. S. *Inorg. Mater* **2001**, *37*, 871-885. DOI: https://doi.org/10.1023/A:1011625728803
15. Steiner, T. *Cryst. Rev*. **1996**, *6*, 1-57. DOI: https://doi.org/10.1039/B313104A
16. Taylor, R.; Kennard, O. *J. Am. Chem. Soc.* **1982**, *104*, 5063-5070. DOI: https://doi.org/10.1021/ja00383a012
17. Lakshmi, B.; Smuelson, A. G.; Jovan Jose, K. V.; Gadre, S. R.; Arunan, E. *New J. Chem.* **2005**, *29*, 371-377. DOI: https://doi.org/10.1039/B411815D
18. Arunan, E.; Desiraju, G. R.; Kein, R. A.; Sadlej, J.; Scheiner, S.; Alkorta, I.; Clary, D. C.; Crabtree, R. H.; Dannenberg, J. J.; Hobza, P.; Kjaergaard, H. G.; Legon, A. C.; Mennucci, B.; Nesbitt, D. J. *Pure Appl. Chem.* **2011**, *83*, 1619-1636. DOI: https://doi.org/10.1351/PAC-REP-10-01-01
19. Bader, R. F. W. *Chem. Rev*. **1991**, *91*, 893-828. DOI: https://doi.org/10.1021/cr00005a013
20. Bader, R. F. W. *J. Phys. Chem. A* **1998**, *102*, 7314-7323. DOI: https://doi.org/10.1021/jp981794v
21. Fuster, F.; Silvi, B. *Theor. Chem. Acc.* **2000**, *104*, 13-21. DOI: https://doi.org/10.1007/s002149900100
22. Burguera, S.; Bauzá, A. *Molecules.* **2024**, *29*, 5606. DOI: https://doi.org/10.3390/molecules29235606
23. Messali, M.; Jhaa, G; Alrashdi, A. A.; Lee, H.-s., Kaya, S.; Sabik, A.; Abualrejal, M. M. A.; Lgaz, H. *Results Phys.* **2025**, *75*, 108331. DOI: https://doi.org/10.1016/j.rinp.2025.108331
24. Panja, S. K.; Kumar, S.; Haddad, B.; Patel, A. R.; Villemin, D.; Amine, H.-M.; Bera, S.; Debdab, M. *Physchem.* **2024**, *4*, 369–388.DOI: https://doi.org/10.3390/physchem4040026
25. Koch, U.; Popelier, P. L. A. *J. Phys. Chem*. **1995**, 99, 9747-9754. https://doi.org/10.1021/j100024a016
26. Lu, T.; Chen, Q. *Comprehensive Computational Chemistry.* 2024, *2*, 240-264. DOI: https://doi.org/10.1016/B978-0-12-821978-2.00076-3
27. Crystallographic Data Centre: Cambridge, UK, 2024. https://www.ccdc.cam.ac.uk
28. Frisch, M. J.; Trucks, G. W.; Schlegel, H. B.; et al. Gaussian 03, revisión B.04; Gaussian Inc.: Pittsburgh, PA, 2003.
29. Keith, T. A. AIMALL, versión 19.10.12; TK Gristmill Software: Overland Park, KS, 2019.
30. Lu, T.; Chen, F. *J. Comput. Chem.* **2012**, *33*, 580-592. DOI: https://doi.org/10.1002/jcc.22885
31. Meng, E. C.; Goddard, T. D.; Pettersen, E. F.; Couch, G. S.; Pearson, Z. J.; Morris, J. H.; Ferrin, T. E. *Protein Sci.* **2023**, *32*, e4792. DOI: DOI: https://doi.org/10.1002/pro.4792
32. Love, I. *J. Phys. Chem. A* **2009**, *113*, 2640-2646. DOI: https://doi.org/10.1021/jp8106183
33. Hernández-Trujillo, J.; Bader, R. F. W. *J. Phys. Chem. A* **2000**, *104*, 1779-1794. DOI: https://doi.org/10.1021/jp994096z
34. Bader, R. F. W.; Matta, C. F. *Organometallics.* **2004**, *23*, 6253-6263. DOI: https://doi.org/10.1021/om049450g
35. Vázquez-Tato, M. P.; Seijas, J. A.; Meijide, F.; de Frutos, S.; Vázquez-Tato, *J. Int. J. Mol. Sci*. **2023**, *24*, 5359. DOI: https://doi.org/10.3390/ijms24065359
36. Mata, I.; Alkorta, I.; Molis, E.; Espinosa, E. *Chem. Eur. J.* **2010**, *16*, 2442-2452. DOI: https://doi.org/10.1002/chem.200901628
37. Fradera, X.; Austen, M. A.; Bader, R. F. W. *J. Phys. Chem. A* **1999**, *103*, 304-314. DOI: https://doi.org/10.1021/jp983362q
38. Johnson, E. R.; Keinan, S.; Mori-Sánchez, P.; Contreras-García, J.; Cohen, A. J.; Yang, W. *J. Am. Chem. Soc.* **2010**, *132*, 6498-6506. DOI: https://doi.org/10.1021/ja100936w
39. Gatti, C.; Cargnoni, F.; Bertini, L. *J. Comput. Chem.* **2003**, *24*, 422-436. DOI: https://doi.org/10.1002/jcc.10205
40. Gatti, C. *Struct. Bonding* **2012**, *147*, 193-286. DOI: https://doi.org/10.1007/430_2010_31
41. Becke, A. D.; Edgecombe, K. E. *J. Chem. Phys*. **1990**, *92*, 5397- 5403. DOI: https://doi.org/10.1063/1.458517

J. Mex. Chem. Soc. **2026**, *70(1):e2576*
Regular Issue

ISSN-e 2594-0317

42. Fuster, F.; Grabowski, S. J. *J. Phys. Chem. A* **2011**, *115*, 10078-10086. DOI: https://doi.org/10.1021/jp2056859
43. Alikhani, M. E.; Fuster, F.; Silvi, B. Struct. Chem. 2005, 16, 203-210. DOI: https://doi.org/10.1007/s11224-005-4451-z
44. Lu, vT.; Chen, Q. *Chem. :Methods* **2021**, 231-239. DOI: https://doi.org/10.1002/cmtd.202100007
45. Arunan, E.; Desiraju, G. R.; Kein, R. A.; Sadlej, J.; Scheiner, S.; Alkorta, I.; Clary, D. C.; Crabtree, R. H.; Dannenberg, J. J.; Hobza, P.; Kjaergaard, H. G.; Legon, A. C.; Mennucci, B.; Nesbitt, D. J. *Pure Appl. Chem.* **2011**, *83*, 1637-1641. DOI: https://doi.org/10.1351/PAC-REC-10-01-02